Numerical Solutions and Bifurcation Analysis of the Fučik Spectrum

by Michael W. McHenry

A Thesis
Submitted in Partial Fulfillment
of the Requirements for the Degree of
Master of Science
in Mathematics

Northern Arizona University
May 2016

Approved:

_____
John M. Neuberger, Ph.D., Chair

_____
Nándor Sieben, Ph.D.

_____
James W. Swift, Ph.D.

ABSTRACT

NUMERICAL SOLUTIONS AND BIFURCATION ANALYSIS OF THE
FUČIK SPECTRUM.

MICHAEL W. MCHENRY

We use a specialized Newton's method to approximate the Fučik spectrum
solution curves of the negative Laplacian on a real Hilbert space. We include
results for the two parameter differential equation. After computing the
spectrum, we add a nonlinear term and compute bifurcation surfaces.

Contents

List of Figures

vi

Chapter 1

Introduction

We use previously studied numerical methods from [6] and [7] to the 0-Dirichlet boundary value problems associated with the two-parameter equation as follows. Note that there will be 5 different families we will cite throughout the paper. The first set are the 3 equations for which we study the Fučik spectrum (Δ in the following denotes the Laplacian):

PDE :

$$-\Delta u = au^+ + bu^- \qquad \text{on } \Omega \tag{1.1}$$
$$u = 0 \qquad \text{on } \partial\Omega,$$

where $\Omega \subseteq \mathbb{R}^2$, $u^+ = \max\{u, 0\}$ and $u^- = \min\{u, 0\}$.

ODE :

$$u'' + au^+ + bu^- = 0 \qquad \text{on } (0,1) \tag{1.2}$$
$$u(0) = 0 = u(1),$$

where $\Omega \subseteq \mathbb{R}$, $u^+ = \max\{u, 0\}$ and $u^- = \min\{u, 0\}$.

Matrix :

$$Ax = ax^+ + bx^- \qquad \text{on } \mathbb{R}^N, \tag{1.3}$$

where $x \in \mathbb{R}^N$, $A \subseteq \mathbb{R}^{N \times N}$, $x^+ = \max\{x, 0\}$, $x^- = \min\{x, 0\}$.

We begin by finding solutions to the Fučik spectrum for Equations (1.1), (1.2), and (1.3). This leads to the goal of the paper which is to analyze the bifurcations of Equation (1.5) stated below. We use numerical methods on the ODE version of Equation (1.5) (namely Equation (1.4)) to act as a stepping stone to reach our final goal.

ODE with non-linear term :

$$u'' + au^+ + bu^- + u^3 = 0 \qquad \text{on } (0,1) \qquad (1.4)$$
$$u(0) = 0 = u(1),$$

where $\Omega \subseteq \mathbb{R}$, $u^+ = \max\{u, 0\}$ and $u^- = \min\{u, 0\}$.

PDE with non-linear term :

$$\Delta u + au^+ + bu^- + u^3 = 0 \qquad \text{on } \Omega \qquad (1.5)$$
$$u = 0 \qquad \text{on } \partial\Omega,$$

where $\Omega \subseteq \mathbb{R}^2$, $u^+ = \max\{u, 0\}$ and $u^- = \min\{u, 0\}$.

We choose this problem due to the work already done on related boundary valued problems.

Chapter 2 discusses the numerical methods that we will be using throughout this paper. We will start with Newton's method, as well as related methods, until we build up to the definition of the Fučik spectrum. Finally we discuss numerical methods used in [7] which relate directly to the methods for our specific problem.

Chapter 3 includes results for a non-linear boundary-value problem that has previously been studied in [6]. We used this example as a stepping stone to result in a numerical approach to approximating solutions to Equations (1.1) and (1.2) using Equation (1.3).

Chapter 4 includes results for Equation (1.2) and (1.4). Each Equation requires a different objective function and Jacobian to approximate solutions. We apply numerical methods described in Chapter 2 to follow bifurcation branches of Equation (1.4).

Chapter 5 includes results for Equation (1.1) and (1.5). Again, each equation requires a different objective function and Jacobian to approximate solutions, only now we are on the square $\Omega = (0,1)^2 \subseteq \mathbb{R}^2$. Again, we

apply all the numerical methods described in Chapter 2 to follow bifurcation branches of Equation (1.5).

Chapter 6 includes results for follow a particular bifurcation branch from Equation (1.5) in which complications arise as you cross the $a = b$ diagonal. We call it a "cusp catastrophe". Following the branch out of the trivial solution, a secondary bifurcation occurs. We ended our research looking at what happens to this secondary bifurcation when following the Fučik spectrum curve.

Chapter 2

Preliminaries

2.1 Newton's Method

Our numerical approximations for this paper rely heavily on the use of Newton's Method. Newton's Method is a zero-finding algorithm. For the one-dimensional case Newton's method is as follows: Let $f : [a, b] \subset \mathbb{R} \to \mathbb{R}$ be a twice continuously differentiable function on $[a, b]$. Starting with an initial guess $x_0 \in [a, b]$, iterate through the following

$$x_{n+1} = x_n - \frac{f(x_n)}{f'(x_n)}.$$

If $\lim_{n \to \infty} x_n = p$, then $f(p) = 0$ (a root of f). Under certain hypothesis, Newton's Method is guaranteed to converge to a zero of f as described in [1]. This algorithm can be applied to systems of non-linear equations as well. The idea of the algorithm remains unchanged, but we now have an object function $\mathbf{G} : \mathbb{R}^n \to \mathbb{R}^n$ for which we wish to find the zeros of $\mathbf{G}$. The object function $\mathbf{G}$ takes as input a vector $x \in \mathbb{R}^n$ and outputs the vector $(G_1(x), G_2(x), ..., G_m(x))$, where $G_i : \mathbb{R}^m \to \mathbb{R}$ are the component functions of G. Then we calculate the Jacobian of our object function. The Jacobian matrix J_G is the matrix of all first-order partial derivatives of the vector valued function $\mathbf{G}$. More precisely, $J : \mathbb{R}^n \to \mathbb{R}^{m+n}$ is defined as

$$J = \left[\frac{\partial \mathbf{G}_i}{\partial \mathbf{x}_j} \right] = \begin{bmatrix} \frac{\partial G_1}{\partial x_1} & \frac{\partial G_1}{\partial x_2} & \cdots & \frac{\partial G_1}{\partial x_n} \\ \vdots & \vdots & \ddots & \vdots \\ \frac{\partial G_m}{\partial x_1} & \frac{\partial G_m}{\partial x_2} & \cdots & \frac{\partial G_m}{\partial x_n} \end{bmatrix}.$$

The algorithm above then becomes:

$$x_{n+1} = x_n - J^{-1}(x_n)\mathbf{G}(x_n),$$

where J^{-1} is the inverse of the matrix J given above. In practice, we will be solving the linear system $J\chi = \mathbf{G}$ for χ. When using MatLab to solve this system we will use the "mldivide" operator, i.e., $\chi = J\backslash\mathbf{G}$.

2.2 Tangent Newton's method

The method to discuss next is an augmented Newton's method. Consider an object function which depends on some real parameter s, ie, $\mathbf{G} = \mathbf{G}(x, s)$. To achieve an algorithm which can find successive roots on our object function, we will use the tangent Gradient Newton Galerkin Augmented Method discussed in [6], only implemented in function space rather than eigenfunction expansion coefficient space. All algorithms in this paper make use of the fact that our vectors represent function values over a discretized set of space-coordinates (which will be helpful when we change to a two-parameter family).

The tangent augmented Newton's method requires the object function $\mathbf{G} : \mathbb{R}^{n+1} \to \mathbb{R}^{n+1}$ and its Jacobian J_G. With the introduction of the parameter s, we now have $n + 1$ unknowns (n from EQ (1.3) and s), but only n equations. In order to solve this system we append a constraint equation to the objective function (thus changing the Jacobian). We add a constraint $\kappa(x, s) = 0$. Our augmented object function $\tilde{\mathbf{G}} : \mathbb{R}^{n+1} \to \mathbb{R}^{n+1}$ is defined by:

$$\tilde{\mathbf{G}} = \begin{pmatrix} \mathbf{G}_s(x) \\ \kappa(x, s) \end{pmatrix}.$$

Using $\tilde{\mathbf{G}}$ in Newton's method forces each term to be 0, hence approximating a zero to the previously mentioned $\mathbf{G}(x, s)$ that also satisfies the constraint.

For the tangent Newton's method, the constraint $\kappa(x, s) : \mathbb{R}^{n+1} \to \mathbb{R}$ is defined as

$$\kappa(x, s) = v^t(x - x_g, s - s_g),$$

where the guess vector is defined by $x_g = x_{old} + \delta v_x$ and $s_g = s_{old} + \delta v_s$. When appended to our object function, iterations are restricted to the orthogonal hyperplane to v. The vector v is an approximate **tangent direction**. For each approximate point along a given solution curve, one calculates a new
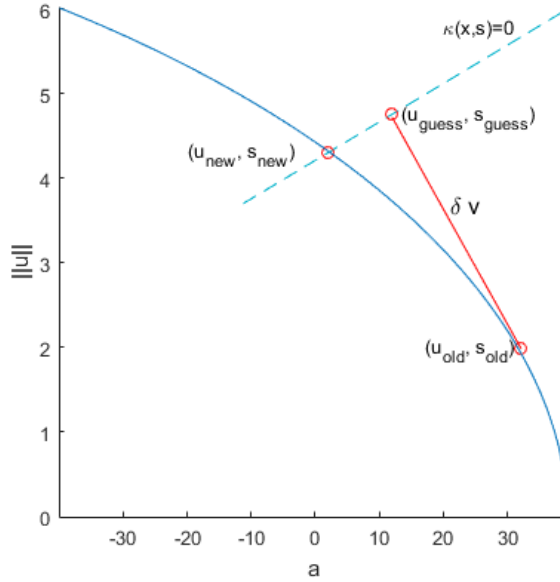
Figure 2.1: One iteration of the tangent Newton's Method.

tangent direction. This tangent direction is computed and normalized every time we converge to a solution pair (u, s), i.e.,

$$v_{new} = \frac{(x_{new} - x_{old}, s_{new} - s_{old})}{||(x_{new} - x_{old}, s_{new} - s_{old})||},$$

where x_{new} is the current approximate point on a solution curve, and x_{old} is from the previous iteration.

2.3   Fučik Spectrum

Let $L : V \to V$ be a self-adjoint operator where V is a real Hilbert space. Consider the equation:

$$Lu = au^+ + bu^-, \tag{2.1}$$

where $u^+ = \max\{u, 0\}$ and $u^- = \min\{u, 0\}$.

Definition 2.3.1 *The* Fučik spectrum *of L is the set of points (a, b) such that Equation (2.1) has a non-trivial solution, called an eigenvector (see [2]).*

6

Theorem 2.3.1 *If u is an eigenvector with parameters (a, b), then $-u$ is an eigenvector with parameters (b, a).*

Proof: Let u be a solution to Equation (2.1) with parameters (a, b). Note that $(-u)^+ = -u^-$ and similarly, $(-u)^- = -u^+$ for any u. Then for $-u$:

$$L(-u) = a(-u^+) + b(-u^-)$$
$$= a(-u)^- + b(-u)^+$$
$$= b(-u)^+ + a(-u)^-.$$

Therefore by Definition 2.3.1, $-u$ is an eigenvector with parameters (b, a). $\square$

2.3.1 A 2x2 Example

Consider $L : \mathbb{R}^2 \to \mathbb{R}^2$ defined by $L(x) = Ax$, where $A = \begin{bmatrix} 2 & -1 \\ -1 & 2 \end{bmatrix}$, which has eigenvalues $\lambda_1 = 1$ and $\lambda_2 = 3$, with corresponding eigenvectors $x_1 = \begin{bmatrix} 1 \\ 1 \end{bmatrix}, x_2 = \begin{bmatrix} 1 \\ -1 \end{bmatrix}$, respectively. For $\lambda_1 = 1$: The eigenvector x_1 has no change in sign. Equation (1.3) becomes

$$A\mathbf{x} = a\mathbf{x} \tag{2.2}$$

since $\mathbf{x}^+ = \mathbf{x}$ and $\mathbf{x}^- = 0$. It is easy to see that $a = 1$ and $b \in \mathbb{R}$ is a solution to Equation (2.2). Similar reasoning will show that $a \in \mathbb{R}$ and $b = 1$ is also in the Fučik spectrum of A. The plotted solutions are a horizontal and vertical line through the point $(1, 1)$.

For $\lambda_2 = 3$: The eigenvector, x_2, has a change in sign, so $x_2^+ = \begin{bmatrix} 1 \\ 0 \end{bmatrix}$ and $x_2^- = \begin{bmatrix} 0 \\ -1 \end{bmatrix}$. Rearranging Equation (2.1) we have

$$Ax - ax^+ - bx^- = 0.$$

Another way to visualize this is by the matrix

$$\begin{bmatrix} 2 - a & -1 \\ -1 & 2 - b \end{bmatrix}. \tag{2.3}$$

To find non-trivial solutions we need to find where $\det(A) = 0$, i.e., solve

$$\begin{vmatrix} 2-a & -1 \\ -1 & 2-b \end{vmatrix} = 0$$

for a, obtaining the curve defined by

$$(2-a)(2-b) = 1, \tag{2.4}$$

which is in the Fučik spectrum of A. This curve is a hyperbola that passes through $(3,3)$ with asymptotes $a = 2$ and $b = 2$. The eigenvalue pairs are depicted in Fig. 2.2.

To verify that we have found all the curves in the Fučik spectrum of A, we start by solving Equation (2.4) for b. Now substitute $b = \frac{2a-3}{a-2}$ into Equation (2.3), which results in the matrix

$$\begin{bmatrix} 2-a & -1 \\ -1 & \frac{1}{2-a} \end{bmatrix}.$$

This results in the eigenvector $\begin{bmatrix} 1 \\ 2-a \end{bmatrix}$. For $a > 2$, clearly $2 - a < 0$. It can be easily verified that

$$\begin{bmatrix} 2 & -1 \\ -1 & 2 \end{bmatrix} \begin{bmatrix} 1 \\ 2-a \end{bmatrix} = a \begin{bmatrix} 1 \\ 0 \end{bmatrix} + \frac{2a-3}{a-2} \begin{bmatrix} 0 \\ 2-a \end{bmatrix}.$$

For $a < 2$, notice that the eigenvector $\begin{bmatrix} 1 \\ 2-a \end{bmatrix}$ contains positive, real numbers. Therefore this is an eigenvector to Equation (2.2) and hence $a = 1$ which implies $b = 1$. So while there is a piece of the hyperbola defined in Equation (2.4) that intersects the point $(1,1)$, only the point $(1,1)$ is in the Fučik spectrum of A. This example is also worked out in [5].

2.4 Solving Elliptical Differential Equations using Numerical Methods

In order to numerically approximate solutions to Equation (1.2) we use the 3-point central second difference to approximate the second derivative. First divide the interval of interest, $[0,1]$ for the ODE, into $n+1$ equal distant meshpoints. For the ODE let $x_i = ih$ with $x_0 = 0$, $x_{n+1} = 1$, and $h =$
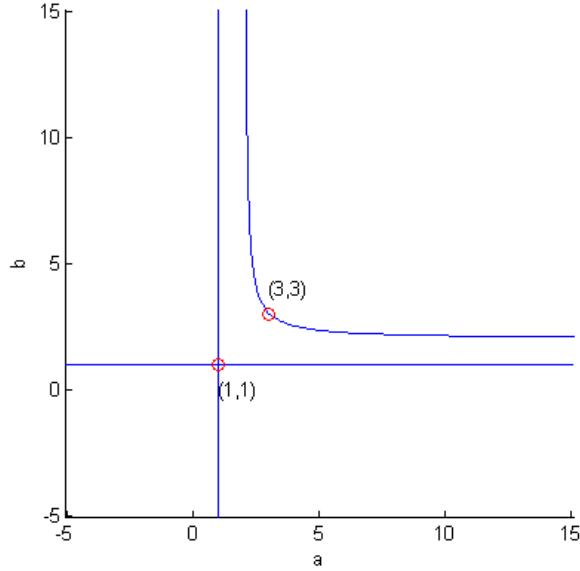
Figure 2.2: Fučik Spectrum of A.

$x_{i+1} - x_i$. We truncate the endpoints to make calculations easier since we have 0-Dirichlet boundary conditions. A regular discretization of a vector $\hat{u} = (u(x_i))_{i=1}^{n-1} \in \mathbb{R}^{n-1}$, where $u : [0,1] \to \mathbb{R}$ for the ODE, will have an approximate second derivative defined by

$$u''(x_i) \approx \frac{u_{i-1} - 2u_i + u_{i+1}}{h^2},$$

as described in [1].

We define the second order central second difference tridiagonal matrix $\tilde{D}_2$ by

$$\tilde{D}_2 = \begin{bmatrix} -2 & 1 & 0 & \dots & & 0 \\ 1 & -2 & 1 & 0 & & \vdots \\ 0 & 1 & -2 & 1 & \ddots & \\ \vdots & \ddots & \ddots & \ddots & \ddots & 0 \\ & & 0 & 1 & -2 & 1 \\ 0 & \dots & & 0 & 1 & -2 \end{bmatrix}.$$

9

Finally, we define

$$D_2 = \frac{1}{h^2} \tilde{D}_2. \tag{2.5}$$

The $(n-1) \times (n-1)$ matrix D_2 enforces 0-Dirichlet boundary conditions. Thus, for $\hat{u} = (g(x_i))_{i=1}^{n-1}$, $D_2\hat{u} \in \mathbb{R}^{n-1}$ is a vector consisting of approximate second derivatives of $\hat{u}$ for use in Equation (1.2).

For Equation (1.1), with $\Omega = (0,1)^2$, $D_{2_{PDE}}$ is a block tridiagonal matrix which approximates the Laplacian by taking x differences within each block and y differences across each block. We discretize the square $(0,1)^2$ into $(n+1)^2$ equally distant gridpoints denoted (x_i, y_j) where $x_i = ih$ and $y_j = jh$ for h as described above. Then for $u : [0,1]^2 \to \mathbb{R}^2$, let the regular discretization be defined by $u_{ij} = u(x_i, y_j)$. First we reshape $\hat{u}$ into a $(n-1)^2 \times 1$ column vector:

$$\hat{u} = \begin{bmatrix} u_{11} \\ \vdots \\ u_{1n-1} \\ u_{21} \\ \vdots \\ u_{n-1,n-1} \end{bmatrix}.$$

We define the $(n-1) \times (n-1)$ matrix T by:

$$T = \begin{bmatrix} -4 & 1 & 0 & \cdots & & 0 \\ 1 & -4 & 1 & 0 & & \vdots \\ 0 & 1 & -4 & 1 & \ddots & \\ \vdots & \ddots & \ddots & \ddots & \ddots & 0 \\ & & 0 & 1 & -4 & 1 \\ 0 & \cdots & & 0 & 1 & -4 \end{bmatrix}.$$

Let I be the $(n-1) \times (n-1)$ identity matrix. Our new $(n-1)^2 \times (n-1)^2$

matrix D_2 for the PDE is:

$$\tilde{D}_{2_{PDE}} = \begin{bmatrix} T & I & 0 & \dots & & 0 \\ I & T & I & 0 & & \vdots \\ 0 & I & T & I & \ddots & \\ \vdots & \ddots & \ddots & \ddots & \ddots & 0 \\ & & 0 & I & T & I \\ 0 & \dots & & 0 & I & T \end{bmatrix},$$

where $D_{2_{PDE}}$ is again given by $D_{2_{PDE}} = \frac{1}{h^2}\tilde{D}_{2_{PDE}}$. That is,

$$(\Delta u)(x_i, y_j) \approx \frac{u_{i-1,j}}{h^2} - \frac{2u_{i,j}}{h^2} + \frac{u_{i+1,j}}{h^2} + \frac{u_{i,j-1}}{h^2} - \frac{2u_{i,j}}{h^2} + \frac{u_{i,j+1}}{h^2}.$$

Simplifying results in the vector $D_2\hat{u} \in \mathbb{R}^{(n-1)^2}$.

2.5   Basis of eigenfunctions

Recall that the negative Laplacian has eigenvalues satisfying

$$0 < \lambda_1 < \lambda_2 \leq \lambda_3 \leq \dots \to \infty,$$

with corresponding eigenfunctions Ψ_j satisfying $-\Delta\Psi_i = \lambda_i\Psi_i$.
For the ODE, Equation (1.2), the single-indexed eigenvalues and corresponding eigenfunctions of the negative second derivative are

$$\begin{aligned} \lambda_j &= j^2\pi^2, \\ \Psi_j(x) &= \sin(j\pi x). \end{aligned} \tag{2.6}$$

For Equation (1.1) the doubly indexed eigenvalues and corresponding eigenvectors of $-\Delta$ are

$$\begin{aligned} \lambda_{j,k} &= (j^2 + k^2)\pi^2, \\ \Psi_{j,k}(x, y) &= \sin(j\pi x)\sin(k\pi x). \end{aligned} \tag{2.7}$$

2.6   Following a bifurcation branch

When following a bifurcation branch using Equation (1.4) or (1.5) we need a convenient way to plot since $u \in \mathbb{R}^{n-1}$. We need an alternate way of

representing its value by a single, real number. Any function, $h : \mathbb{R}^{n-1} \to \mathbb{R}$, is what we call a *schematic function*. Our choice for this paper is the ∞-norm of u. Since the function u is a discretized, i.e., $u = (u_1, u_2, ..., u_{n-1})$:

$$||\hat{u}||_\infty = \max\{|u_1|, |u_2|, ..., |u_{n-1}|\}.$$

Refer to Figure 3.1 as an example of plotting bifurcation branches using the ∞-norm.

Chapter 3

Example

3.1 Non-linear BVP

We begin by presenting the numerical methods of [7] which are used to
find solutions to a single parameter ODE with 0 Dirichlet boundary condi-
tions. Adaptations of these methods will apply to the two-parameter Equa-
tion (1.1). Consider these numerical methods to the family of BVP

$$y'' + sy + y^3 = 0 \qquad \text{on } (0,1) \tag{3.1}$$
$$y = 0 \qquad \text{on } \partial(0,1).$$

Here, s is a single, real-valued bifurcation parameter.

When $|y| \ll 1$, the equation is dominated by the linear eigenvalue equa-
tion $y'' + sy = 0$ with 0-Dirichlet boundary conditions. The non-trivial
solutions take the form $\Psi_k(x) = \sin(k\pi x)$ with corresponding eigenvalues
$s_k = k^2\pi^2$. At each point s_k along the trivial branch, the Jacobian of $\mathbf{G}$ is
non-invertible. This tells us that there is a 0 eigenvalue. The Implicit Func-
tion Theorem tells us that these are the points at which bifurcation can occur.
At these points, $k^2\pi^2$, we "look" in the eigenvector direction corresponding
to the 0 eigenvalue, i.e.,

$$v = \Psi_k,$$

and then run tangent Newton's method. First discretize x into $n+1$ equidis-
tant gridpoints $\Omega = (0,1)$, as in Section 2.4, and let $\hat{y} = y(x_i)_{i=1}^{n-1}$. Our object
function $\mathbf{G} \in \mathbb{R}^N$ for tangent Newton's method is

$$\mathbf{G} = \left[D_2\hat{y} + s\hat{y} + \hat{y}^3 \right].$$
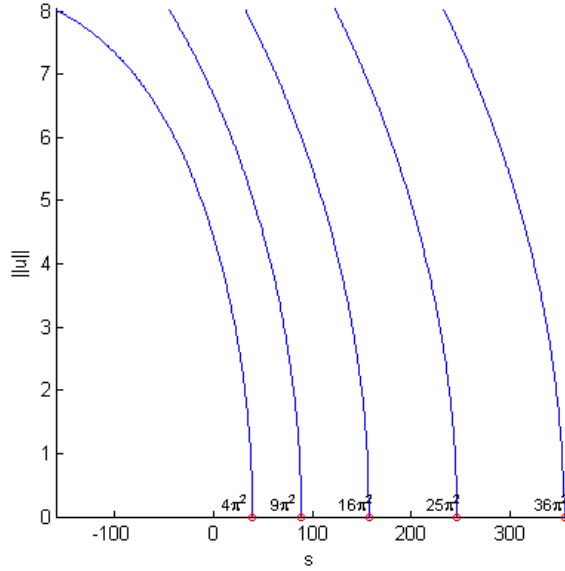
13

Figure 3.1: Bifurcation branches from the first 5 bifurcation points.

Note that $\hat{y}^3$ is evaluated component-wise, that is $(\hat{y}^3)_i = \hat{y}_i^3$.

Figure 3.1 depicts our approximations of the bifurcation branches out of the points s_k for $k \in \{1, ..., 5\}$. We will use these points as initial values for our approximations to the Fučik spectrum.

Chapter 4

Fučik Spectrum for the ODE.

4.1 Approximating the Fučik spectrum for the ODE.

Consider Equation (1.2). When $a = b$, this is the eigenvalue problem with solutions given in Equation (2.6). We know that the bifurcation points that lie on the $a = b$ diagonal for the trivial solution occur at $k^2\pi^2$ for $k \in \mathbb{N}$, with corresponding eigenvectors $\Psi_k = \sin(k\pi x)$. Our object function is

$$\tilde{\mathbf{G}} = \begin{bmatrix} D_2\hat{u} + a\hat{u}^+ + b\hat{u}^- \\ (1 - \hat{u} \cdot \hat{u})/2 \\ \kappa(\hat{u}, a, b) \end{bmatrix}.$$

The first equation, $D_2\hat{u} + a\hat{u}^+ + b\hat{u}^- = 0$, is a discretized version of Equation (1.3). We introduced tangent Newton's method in Chapter 2, but we only had one variable. To account for the second variable we add another equation to solve the system. The second equation is to assure us that our eigenvector $\hat{u}$ maintains a norm of 1. Notice that any positive multiple of an eigenfunction solution will still satisfy Equation (1.3). The constant 1 in $(1 - \hat{u} \cdot \hat{u})$ here is an arbitrary choice. We use a similar concept for $\kappa(\hat{u}, a, b)$ as discussed in Section 2.2, i.e.,

$$\kappa(\hat{u}, a, b) = v^t(\hat{u} - \hat{u}_g, a - a_g, b - b_g).$$
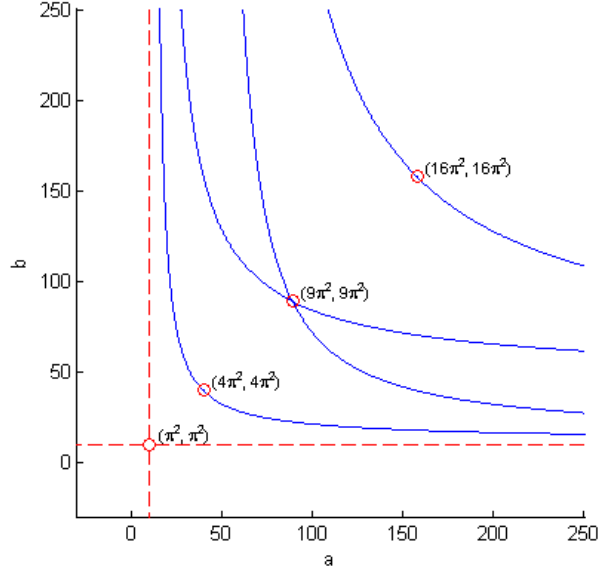
15

Figure 4.1: The approximate solutions to the Fučik spectrum through the points (λ_1, λ_1), (λ_2, λ_2), (λ_3, λ_3) and (λ_4, λ_4).

The Jacobian of $\tilde{G}$ is

$$J_G = \begin{bmatrix} D_2 + \operatorname{diag}(a\chi_{\{x|x>0\}} + b\chi_{\{x|x<0\}}) & \hat{u}^+ & \hat{u}^- \\ -\hat{u}^t & 0 & 0 \\ v^t & & \end{bmatrix}.$$

Finally we define our initial guess point as $(\pm \sin(k\pi x), k^2\pi^2, k^2\pi^2)$ and the initial search direction as

$$\hat{v} = \pm \begin{bmatrix} 0 \\ \vdots \\ 0 \\ 1 \\ -1 \end{bmatrix}.$$

The approximate solutions to the Fučik spectrum for Equation (1.2) through the points (λ_1, λ_1), (λ_2, λ_2), (λ_3, λ_3) and (λ_4, λ_4) are plotted in Figure 4.1.
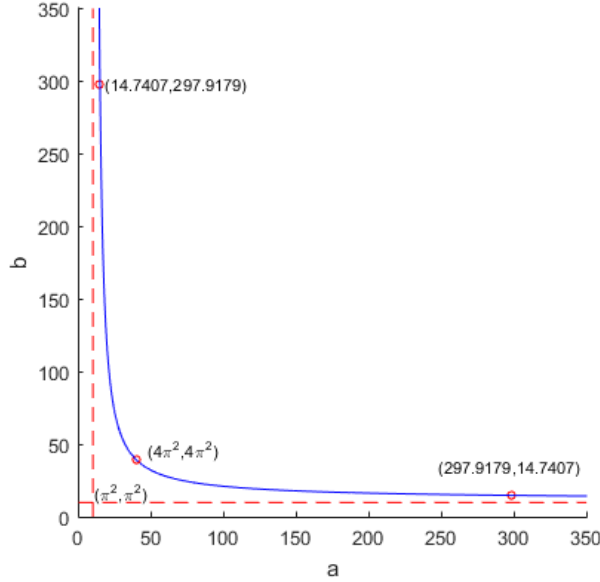
Figure 4.2: Fučik spectrum for Equation (1.2) that passes the point (λ_2, λ_2).

4.2 How does the solution change along the Fučik spectrum?

Consider the solution curve in the spectrum that intersects (λ_2, λ_2), which has the corresponding eigenvector Ψ_2. Figure 4.3 depicts how the solution, $\hat{u}$, changes along the Fučik spectrum which pass through the point λ_2 in Figure 4.2.

As the parameter a increases, parameter b decreases to satisfy Equation (1.2). We also look at how solutions change along the Fučik spectrum which passes through the point λ_3 depicted in Figures 4.4 and 4.5.

4.2.1 Multiple solution curves through a single eigenvalue

Symmetry of the eigenfunctions allow for multiple solution curves through a known bifurcation value, i.e., $\lambda_k = k^2\pi^2$. It is only the solution curves through the eigenvalues λ_{2k-1} for all $k \in \mathbb{N}$ that have two curves you can see with our choice of schematic function h.
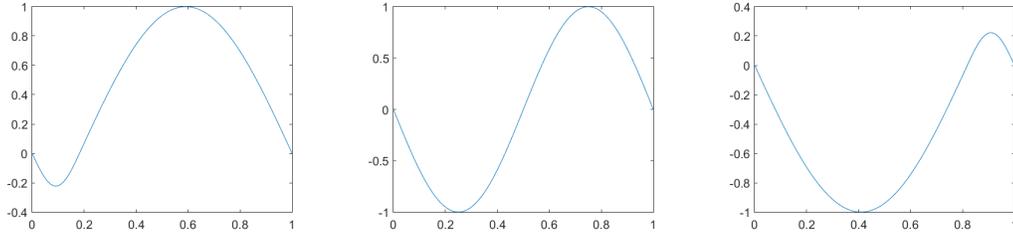
17

Figure 4.3: Approximate solution $\hat{u}$ are depicted at the points $(14.7404, 297.9179)$, $(4\pi^2, 4\pi^2)$, and $(297.9179, 14.7407)$ from Figure 4.2 respectively.

Consider the Fučik spectrum that curves through $\lambda_3 = 9\pi^2$, plotted in Figure 4.4.

Notice how the left eigenvector solution in Figure 4.5 is approaching what looks like $|\sin(2\pi x)|$ as $b \to \infty$ which corresponds to a vertical asymptote at $a = 4\pi^2$, i.e., the value of λ_2 which has corresponding eigenfunction $\sin(2\pi x)$. The right eigenvector solution indicates that as $a \to \infty$ the solution approaches $-\sin(\pi x)$. Again, this appears to have a horizontal asymptote at $b = \pi^2$ which should also look familiar (it is the value of λ_1 which has corresponding eigenfunction $\sin(\pi x)$).

4.3 Bifurcation analysis for the ODE

Consider Equation (1.4). We have seen how to follow the solution curves in the (a, b) plane, we turn our focus towards adding a non-linear term. It can be shown that along the curve in Figure (4.1) the Jacobian of $\tilde{G}$ is non-invertible. As stated before, theory tells us that bifurcation is a possible reason why our Jacobian of $\tilde{G}$ is non-invertible [6].

In order to follow a bifurcation surface, we no longer use the constraint $(1 - \hat{u} \cdot \hat{u})/2$. After removing this constraint, we have n equations and $n + 1$ unknowns. To resolve this we came up with a scheme to follow a segment of the surface (we call it a bifurcation branch) which is restricted to lines parallel to the $a = b$ diagonal line. This allows the parameter a to be treated as a variable, as before, and now the parameter b depends on a. Namely we follow bifurcation branches along the $b = a + c$ line.
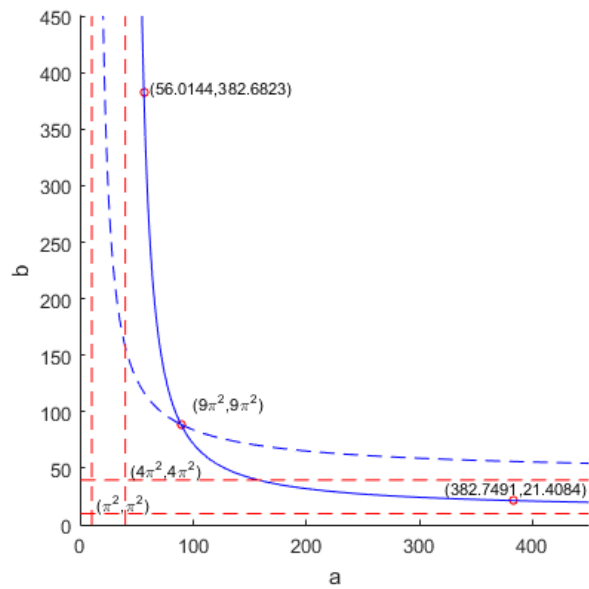
18

Figure 4.4: Fučik spectrum for Equation (1.2) that passes through the point (λ_3, λ_3). The solid curve corresponds to $\hat{u} = \sin(3\pi x)$ and the dashed lined corresponds to $\hat{u} = -\sin(3\pi x)$. Horizontal asymptotes at $b = \pi^2, 4\pi^2$ and veritcal asymptotes at $a = \pi^2, 4\pi^2$ are also depicted.
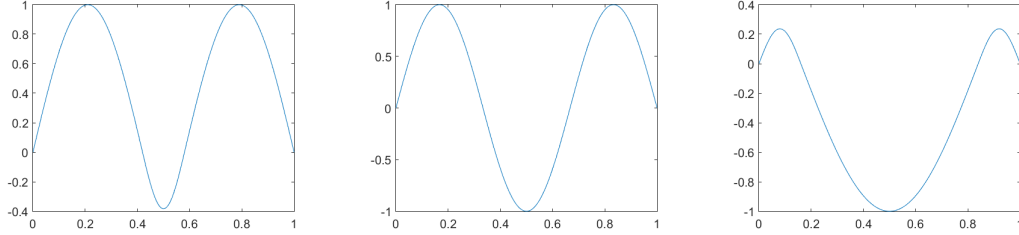
Figure 4.5: Approximate solution $\hat{u}$ is depicted at the points $(56.0144, 382.6823)$, $(9\pi^2, 9\pi^2)$, and $(382.7491, 21.4084)$ along the solid curve in Figure 4.4 respectively.

Our new object function becomes

$$\tilde{\mathbf{G}} = \begin{bmatrix} D_2\hat{u} + a\hat{u}^+ + (a+c)\hat{u}^- + \hat{u}^3 \\ \kappa(\hat{u}, a) \end{bmatrix},$$

with Jacobian

$$J_G = \begin{bmatrix} -D_2 + \mathrm{diag}(a\chi_{\{x|x>0\}} + (a+c)\chi_{\{x|x<0\}}) + \mathrm{diag}(3\hat{u}^2) & \hat{u} \\ v^t \end{bmatrix}.$$

Our search direction $\hat{v}$ changes now that we have one less variable. We use the eigenvector at the current bifurcation point as our search direction, i.e.,

$$\hat{v} = \begin{bmatrix} \hat{u} \\ 0 \end{bmatrix} \in \mathbb{R}^n.$$

We start at the point $(a, a+c)$ and $\hat{u} = 0$ in the Fučik spectrum. The guess for the next point for tangent Newton's method is $\begin{bmatrix} 0 \\ a \end{bmatrix} + \delta \begin{bmatrix} \hat{u} \\ 0 \end{bmatrix}$.

4.4 How do solutions change along bifurcation branches?

Again, let's consider the solution to Equation (1.2) whose Fučik spectrum passes through the point (λ_2, λ_2). Since Equation (1.4) has a superlinear term, we know our positive and negative components will be "stretched" in their respective directions. Intuition tells us that the parameters a and b
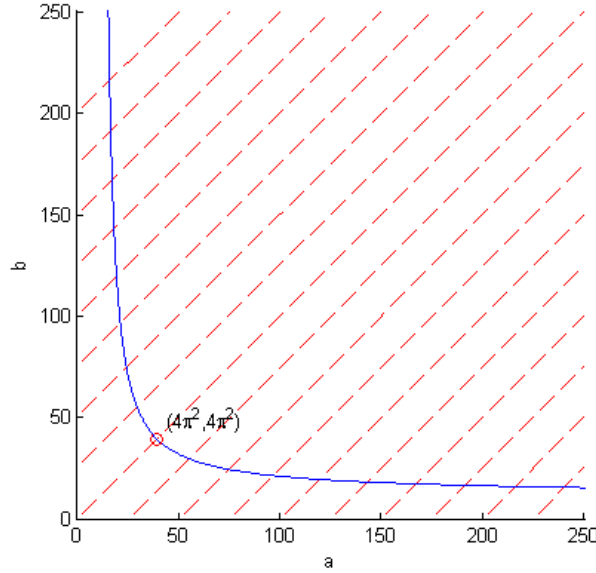
Figure 4.6: To follow a branch on the bifurcation surface we restrict our solutions to Equation (1.4) to lines of the form $b = a + c$ which are parallel to $a = b$.

must be a lot smaller in order for Equation (1.4) to be satisfied. Let's look at what happens to solution u as we follow one of these branches (specifically the one out of the point (λ_2, λ_2) in Figure 4.7).

The branch bifurcating from the point $(4\pi^2, 4\pi^2)$ using Equation (1.4) is depicted in Figure (4.7).

If we continued to follow this branch, our solutions would start to "spike". Graphically, if we continued along the branch in Figure 4.7 our solutions start to look like that in Figure 4.9.

Once we have crafted a branch along each diagonal as in Figure 4.6, we combine all the branches together to get one cohesive graphic that represents the bifurcation surface for each curve in the Fučik spectrum. Figure 4.10 depicts the bifurcation curves for the solutions whose Fučik spectrum curves pass through the points (λ_2, λ_2) and (λ_3, λ_3).
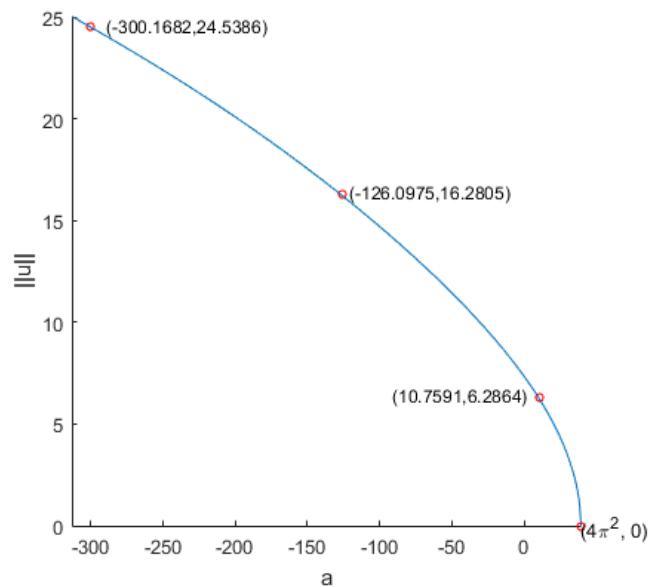
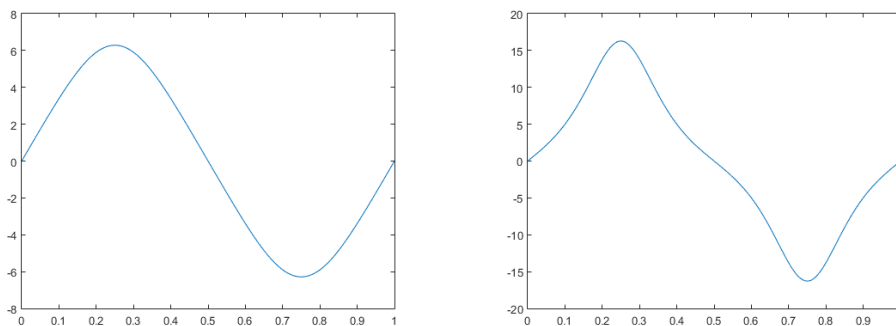Figure 4.7: A sample branch from the point $(4\pi^2, 4\pi^2)$ for Equation (1.4).

Figure 4.8: Approximate solutions $\hat{u}$ are depicted at the points $(10.7591, 6.2864)$ and $(-126.0975, 16.2805)$ from Figure 4.7, respectively.
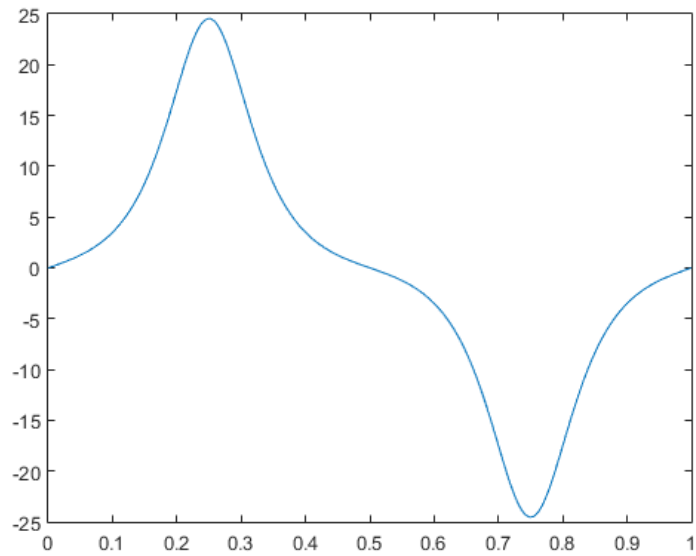
22

Figure 4.9: Solution u to Equation (1.4) at the point $(-300.1682, 24.5386)$ on a bifurcation branch in Figure 4.7.
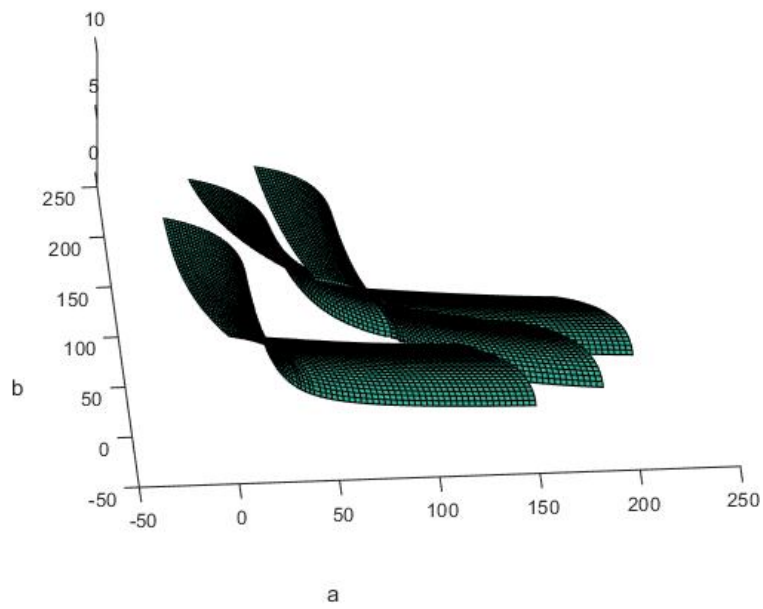
Figure 4.10: Bifurcation surfaces of Equation (1.4) for the Fučik spectrum curves which pass through the points (λ_2,λ_2) and (λ_3,λ_3).

Chapter 5

The Fučik Spectrum for the PDE.

Now we consider Equation (1.1). Our approximated solution vector $\hat{u}$ will now be an $(n-1) \times (n-1)$ matrix instead of an $(n-1) \times 1$ vector as was the case for the ODE. In order for the tangent Newton's method to function properly we need to resize $\hat{u}$ to a $(n-1)^2 \times 1$ column vector. We use the "reshape" command in MatLab to accomplish this.

5.1 The symmetries of eigenfunctions for the PDE

Let $\mathbf{D}_4$ be the symmetry of the square $\Omega = (0,1) \times (0,1)$, which is generated by 2 involutions:

$$\mu \cdot (x,y) = (1-x,y) \text{ and } \delta \cdot (x,y) = (y,x).$$

If $u(x,y)$ is a solution to Equation(1.1), then so is $\gamma \cdot u(x,y)$ for any $\gamma \in \mathbf{D}_4 = \langle \mu, \delta \rangle$. More detail can be found in [7]. Therefore, at every $\lambda_{j,k} = \lambda_{k,j}$ there are up to 5 possible eigenfunctions we need to consider:

    i. $\Psi_{j,k}$ and $\Psi_{k,j}$

    ii. $\Psi_{j,k} + \Psi_{k,j}$

    iii. $\Psi_{j,k} - \Psi_{k,j}$ and $\Psi_{k,j} - \Psi_{j,k}$

Figures 5.10, 5.2, and 5.3 are depictions of the eigenfunctions for $-\Delta$ on $(0,1)^2$ with 0 Dirichlet boundary conditions. For the first three doubly indexed eigenvalues of $-\Delta$ we will list the distinct symmetries.

- For $\lambda_{1,2} = \lambda_{2,1}$: There are only two distinct symmetries in this subspace. They are depicted in Figure 5.10.

    i. $\Psi_{1,2}$ and $\Psi_{1,2} + \Psi_{2,1}$.

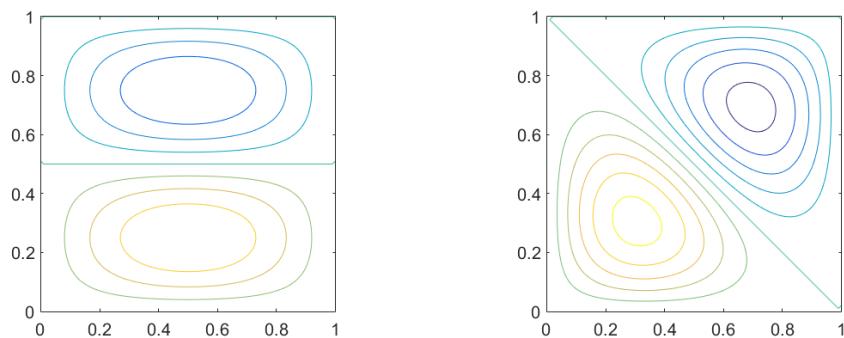

Figure 5.1: Two eigenfunctions of $-\Delta$ on $(0,1)^2$: $\Psi_{1,2}$ and $\Psi_{1,2} + \Psi_{2,1}$.

- $\lambda_{2,2}$ is a simple eigenvalue so there is only one distinct symmetry:

    i. $\Psi_{2,2}$ is depicted in Figure 5.2.

- For $\lambda_{1,3} = \lambda_{3,1}$:
  There are three distinct symmetries in this subspace. They are depicted in Figure 5.3.

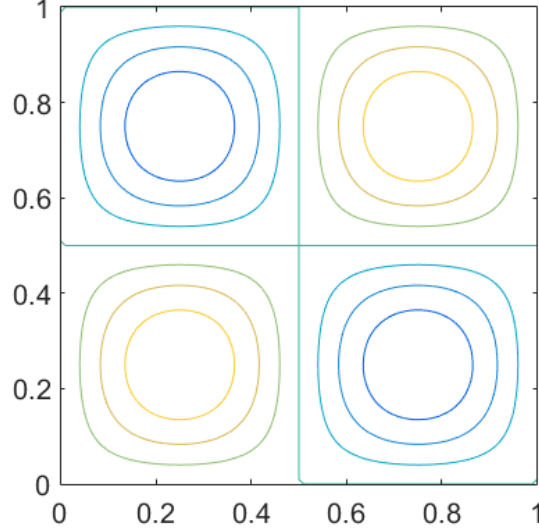   i. $\Psi_{1,3}$, $\Psi_{1,3} + \Psi_{3,1}$, and $\Psi_{1,3} - \Psi_{3,1}$ are depicted in Figures 5.3.

Figure 5.2: The $\Psi_{2,2}$ eigenfunction of $-\Delta$ on $(0,1)^2$.

5.2 Approximating the Fučik spectrum for the PDE.

With our resized vector u as mentioned at the beginning of the chapter, we apply the same method as discussed in Section 4.1. Only now we are using $D_{2_{PDE}}$ to approximate the Laplacian. That is, our object function, $\tilde{\mathbf{G}} \in \mathbb{R}^{(n-1)^2+2}$, is

$$\tilde{\mathbf{G}} = \begin{bmatrix} -D_{2_{PDE}}\hat{u} + a\hat{u}^+ + b\hat{u}^- \\ (1 - \hat{u} \cdot \hat{u})/2 \\ \kappa(a,b,\hat{u}) \end{bmatrix},$$

with Jacobian $J_G \in \mathbb{R}^{(n-1)^2+2} \times \mathbb{R}^{(n-1)^2+2}$, where

$$J_G = \begin{bmatrix} -D_{2_{PDE}} + \mathrm{diag}(a\chi_{\{x|x>0\}} + b\chi_{\{x|x<0\}}) & \hat{u}^+ & \hat{u}^- \\ -\hat{u}^t & 0 & 0 \\ & v^t & \end{bmatrix}.$$

Figure 5.4 shows the Fučik spectrum for the first 3 sign changing solutions which pass through the points $(\lambda_{1,2}, \lambda_{1,2}), (\lambda_{2,2}, \lambda_{2,2})$ and $(\lambda_{1,3}, \lambda_{1,3})$ (refer to Section 2.5). We used all symmetries for each subspace to find the Fučik spectrum which passes through each of the aforementioned points.
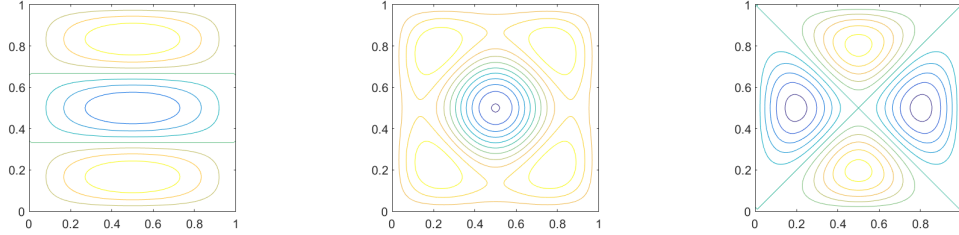
Figure 5.3: Three eigenfunction of $-\Delta$ on $(0,1)^2$: $\Psi_{1,3}$, $\Psi_{1,3}+\Psi_{3,1}$, $\Psi_{1,3}-\Psi_{3,1}$ respectively.

5.3 How do solutions change along the Fučik spectrum?

Figure 5.5 is the Fučik spectrum for Equation (1.1) corresponding to $\Psi_{1,2}$ which pass through the point $(\lambda_{1,2}, \lambda_{1,2})$. As with the ODE, as the parameter a increases, the parameter b decreases to satisfy Equation (1.1). The approximate solution $\hat{u}$ at each point is depicted in Figure 5.6.

We also plot the Fučik spectrum for Equation (1.1) whose curves that pass through the points $(\lambda_{2,2}, \lambda_{2,2})$ and $(\lambda_{1,3}, \lambda_{1,3})$ in Figures 5.7 and 5.9 respectively.

5.4 Bifurcation analysis of the PDE

We used the same method for finding and plotting the bifurcation planes for the PDE as we did for the ODE in Section 4.3 after reshaping our vector $\hat{u}$. We restrict our solutions to lines parallel to the $a = b$ diagonal as depicted in Figure 4.6. Again, we follow a single branch at a time and then mesh the branches together to create the bifurcation surface.

Recall that our object function remains the same as in Section 4.3, only now $\tilde{\mathbf{G}} \in \mathbb{R}^{(n-1)^2+1}$. That is,

$$\tilde{\mathbf{G}} = \begin{bmatrix} -D_{2_{PDE}}\hat{u} + a\hat{u}^+ + (a+c)\hat{u}^- + \hat{u}^3 \\ \kappa(\hat{u}, a) \end{bmatrix},$$
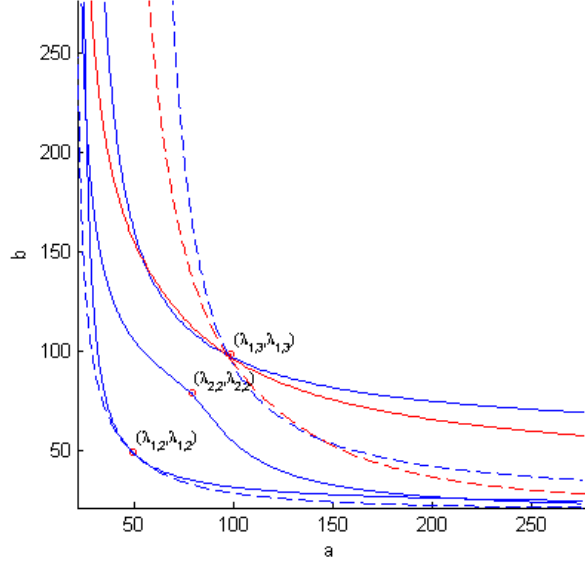
Figure 5.4: The Fučik spectrum for Equation (1.1) whose solutions pass through the points $(\lambda_{1,2}, \lambda_{1,2}), (\lambda_{2,2}, \lambda_{2,2})$, and $(\lambda_{1,3}, \lambda_{1,3})$.

with Jacobian

$$J_G = \begin{bmatrix} -D_{2_{PDE}} + \text{diag}(a\chi_{\{x|x>0\}} + (a+c)\chi_{\{x|x<0\}}) + \text{diag}(3\hat{u}^2) & \hat{u} \\ v^t & \end{bmatrix}.$$

Figure 5.11 depicts the first 3 sign-changing solutions through $(\lambda_{1,2}, \lambda_{1,2})$, $(\lambda_{2,2}, \lambda_{2,2})$, and $(\lambda_{1,3}, \lambda_{1,3})$.

5.5 How do solutions change along a bifurcation branch?

Solutions follow a similar pattern as seen in Section 4.4. The approximated solution $\hat{u}$ stretches as you follow along the bifurcation surface. We will follow the bifurcation branch out of the point $(\lambda_{1,2}, \lambda_{1,2})$ using the eigenvector $\hat{u} = \Psi_{2,1}$ along the $a = b$ diagonal.

The solution which passes through $(\lambda_{1,2}, \lambda_{1,2})$ along the $a = b$ diagonal is already depicted in Figure 5.10. Figure 5.13 depicts how the approximate
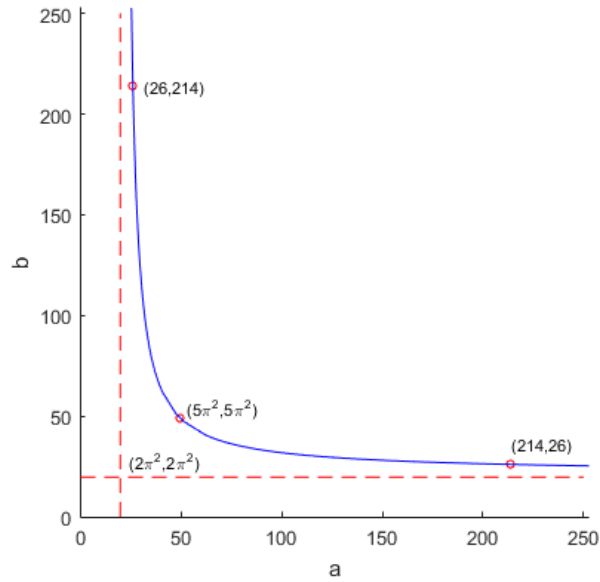
Figure 5.5: The Fučik spectrum for Equation (1.1) corresponding to $\Psi_{1,2}$ which passes through the point $(\lambda_{1,2}, \lambda_{1,2})$. Asymptotes $a = 2\pi^2$ and $b = 2\pi^2$ are also included.

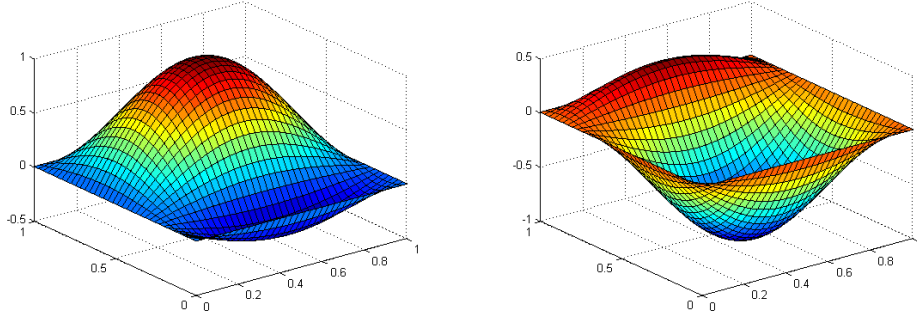solution $\hat{u}$ changes as you follow the bifurcation branch out of the point $(\lambda_{1,2}, \lambda_{1,2})$.

Figure 5.6: Approximate solutions corresponding to $\Psi_{1,2}$ at the points $(26, 214)$ and $(214, 26)$ in Figure 5.5 respectively.
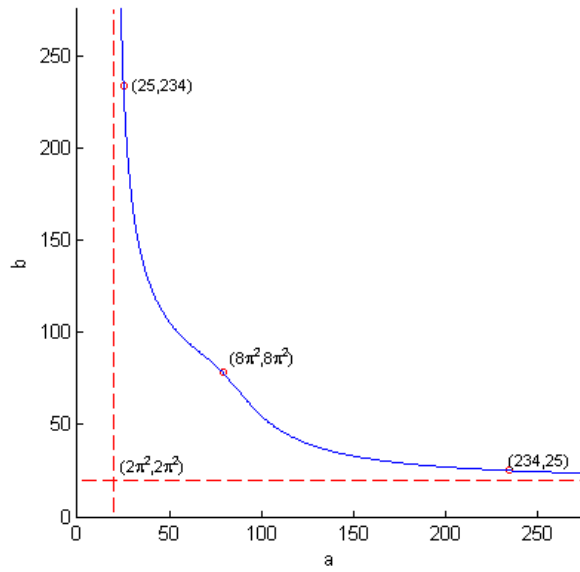

Figure 5.7: The Fučik spectrum for Equation (1.1) which passes through the point $(\lambda_{2,2}, \lambda_{2,2})$. Asymptotes $a = 2\pi^2$ and $b = 2\pi^2$ are also included.
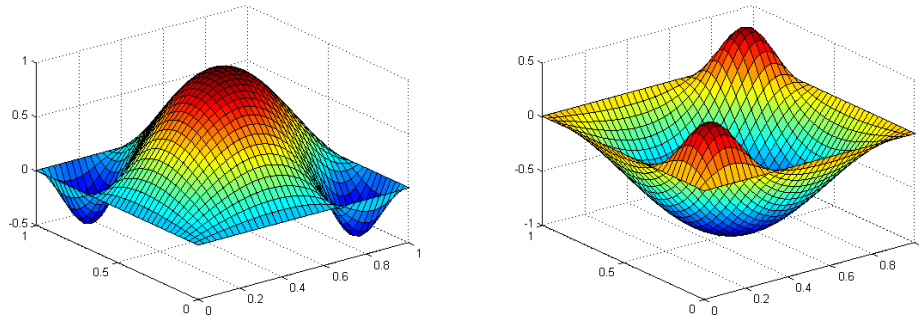
Figure 5.8: Approximate solutions corresponding to $\Psi_{2,2}$ at the points $(25, 234)$ and $(234, 23)$ in Figure 5.7 respectively.
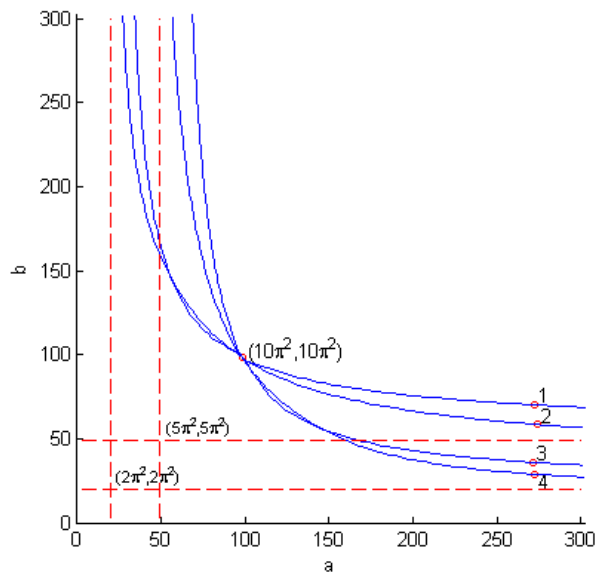

Figure 5.9: The Fučik spectrum for Equation (1.1) which pass through the point $(\lambda_{1,3}, \lambda_{1,3})$. Horizontal asymptotes at $b = \pi^2, 5\pi^2$ and veritcal asymptotes at $a = \pi^2, 5\pi^2$ are also depicted.
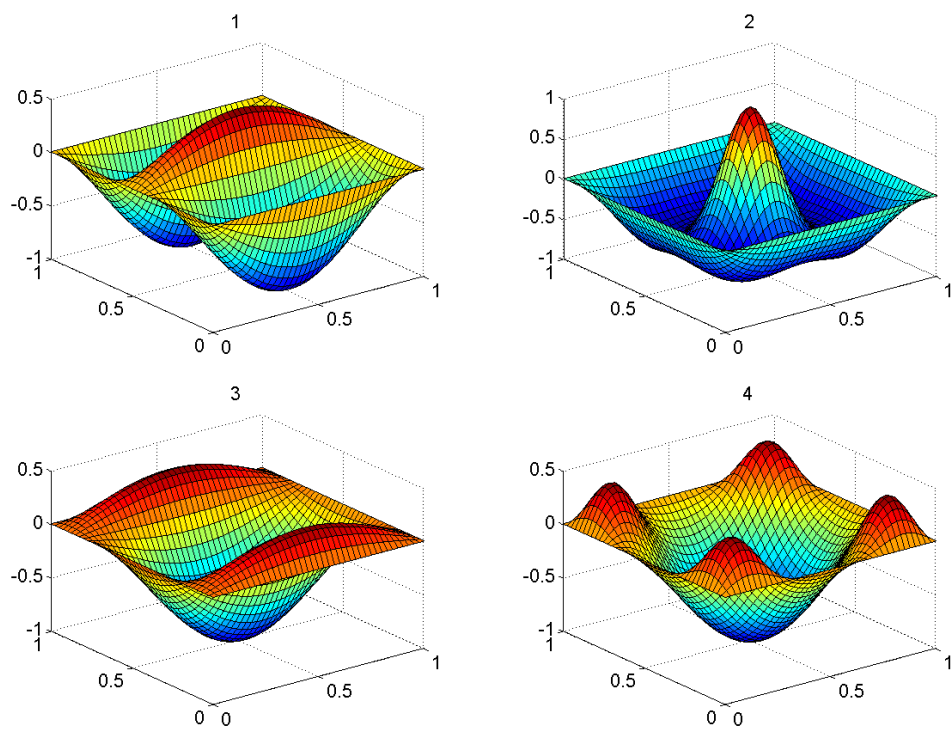
Figure 5.10: Approximate solutions at selected points in the Fučik spectrum labeled in Figure 5.9.
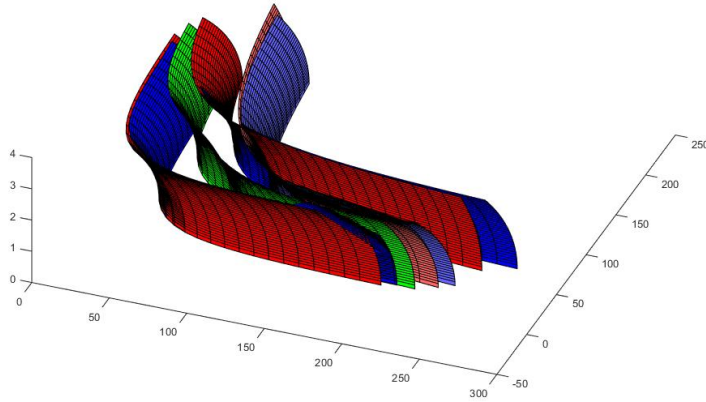
Figure 5.11: Bifurcation surfaces through the first 3 sign-changing solutions for Equation (1.5).
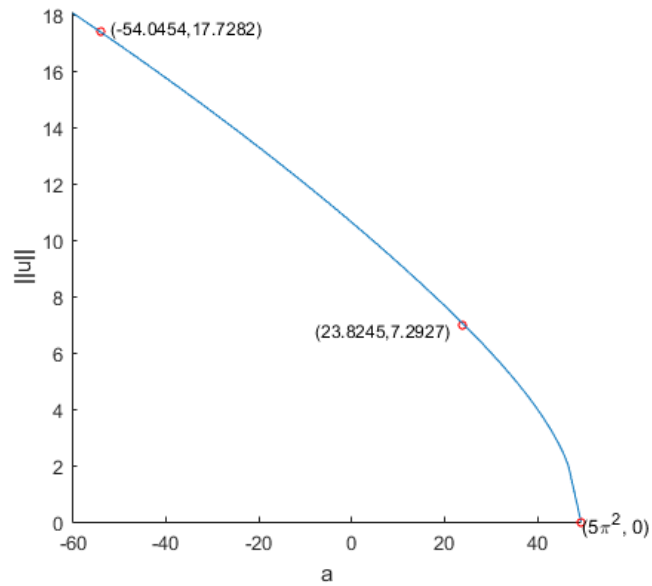

Figure 5.12: A branch out of the point $(\lambda_{1,2}, \lambda_{1,2})$ using $\Psi_{1,2}$ for Equation (1.5).
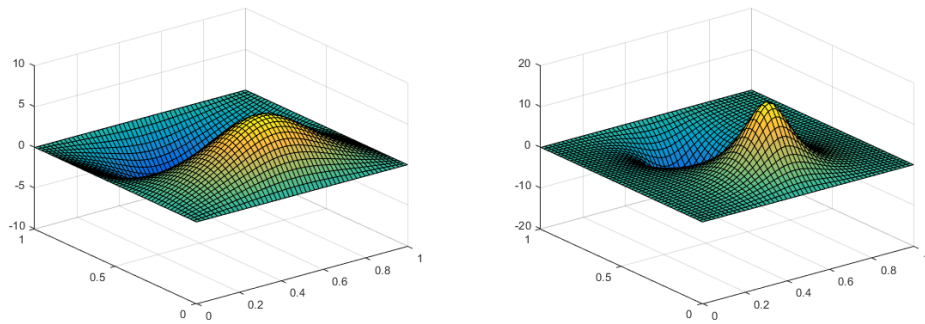
Figure 5.13: How the approximate solution $\hat{u}$ changes as you follow the branch out of the point $(\lambda_{1,2}, \lambda_{1,2})$. They are the solutions at the points $(23.8245, 7.2927)$ and $(-54.0454, 17.7282)$ in Figure 5.12 respectively.

Chapter 6

Current and Future Research

6.1   A cusp catastrophe

We are currently investigating the secondary bifurcations of the $\Psi_{1,3}$ branch out of the point $(\lambda_{1,3}, \lambda_{1,3})$. We know how this bifurcation diagram looks along the $a = b$ diagonal but an interesting thing occur we small perturbations to the left and right. Recall in Chapter 4 that we parameterized b to reduce by one variable. We follow bifurcation branches along the $b = a + c$ lines (Figure 4.6). We have evidence suggesting that a cusp catastrophe is occurring as you move across the $a = b$ diagonal.

Secondary bifurcation depicted in Figure 6.1, 6.2, and 6.3 occur at a point where there is a change in the Morse index of the Hessian, i.e., one of our eigenvalues hit 0. Due to the nature of all this branch splitting, we have had difficulty rendering a smooth bifurcation surface that includes the secondary bifurcations.

6.2   Future Research

We are interested in finding alternative approaches for rendering these bifurcation surfaces. Figures 6.1, 6.2, and 6.3 occur out of one of the 4 Fučik spectrum curves which pass through the point $(\lambda_{1,3}, \lambda_{1,3})$. We suspect a lot more intricacies will occur as we attempt to render multiple branches from different curves out of the a, b-plane.
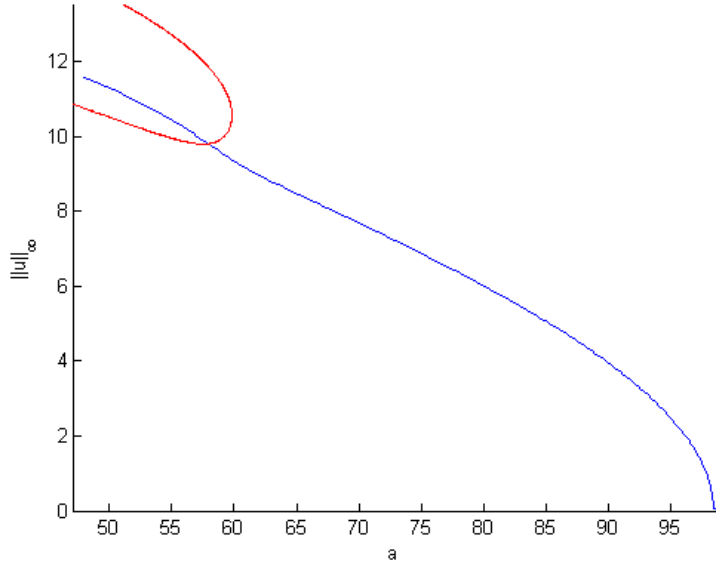
Figure 6.1: Following the $\Psi_{1,3}$ bifurcation branch along the line $b = a - 0.7$.
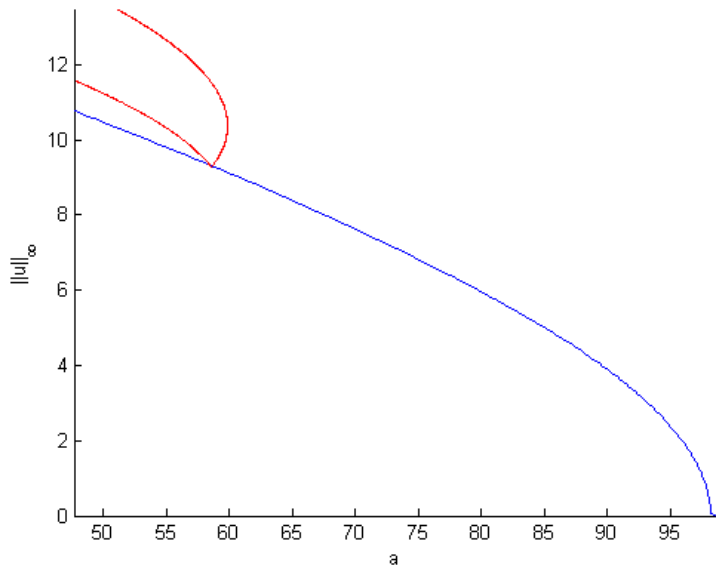

Figure 6.2: Following the $\Psi_{1,3}$ bifurcation branch along the line $a = b$.
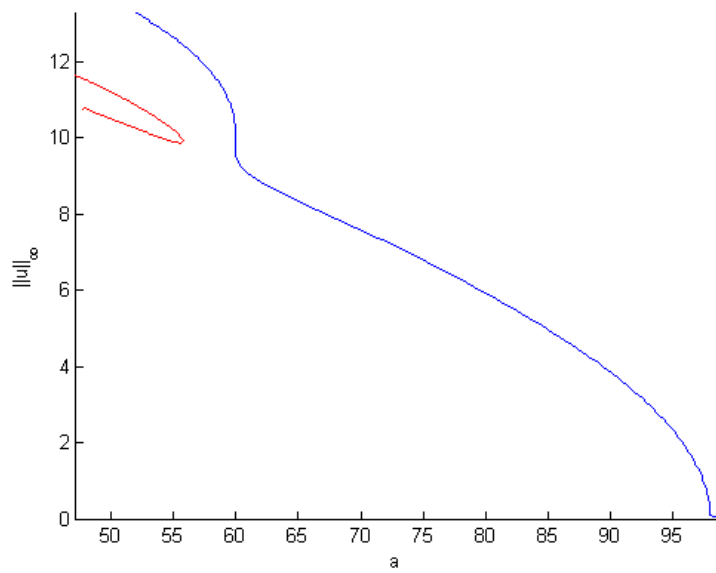
37

Figure 6.3: Following the $\Psi_{1,3}$ bifurcation branch along the line $b = a + 0.5$.

Bibliography

[1] Richard L. Burden and J. Douglas Faires. *Numerical Analysis 9th Ed.* Brooks/Cole, Boston, MA, 2011.

[2] Alfonso Castro and Chen Chang. A variational characterization of the Fucik spectrum and applications. *Rev. Colombiana Mat.*, 44(1):23–40, 2010.

[3] C. Tyler Diggans, John M. Neuberger, and James W. Swift. Symmetry analysis and numerical solutions for semilinear elliptic systems. In *Proceedings of the Variational and Topological Methods: Theory, Applications, Numerical Simulations, and Open Problems*, volume 21 of *Electron. J. Differ. Equ. Conf.*, pages 61–76. Texas State Univ., San Marcos, TX, 2014.

[4] J. Horák and W. Reichel. Analytical and numerical results for the Fučík spectrum of the Laplacian. *J. Comput. Appl. Math.*, 161(2):313–338, 2003.

[5] Caryl Margulies and William Margulies. Nonlinear resonance set for nonlinear matrix equations. *Linear Algebra Appl.*, 293(1-3):187–197, 1999.

[6] John M. Neuberger, Nándor Sieben, and James W. Swift. Automated bifurcation analysis for nonlinear elliptic partial difference equations on graphs. *Internat. J. Bifur. Chaos Appl. Sci. Engrg.*, 19(8):2531–2556, 2009.

[7] John M. Neuberger, Nándor Sieben, and James W. Swift. Newton's method and symmetry for semilinear elliptic PDE on the cube. *SIAM J. Appl. Dyn. Syst.*, 12(3):1237–1279, 2013.

[8] John M. Neuberger and James W. Swift. Newton's method and Morse index for semilinear elliptic PDEs. *Internat. J. Bifur. Chaos Appl. Sci. Engrg.*, 11(3):801–820, 2001.